

# Universal Planckian relaxation in the strange metal state of the cuprates

A. Shekhter,<sup>1,\*</sup> B. J. Ramshaw,<sup>2</sup> M. K. Chan,<sup>1</sup> and N. Harrison<sup>1</sup>

<sup>1</sup>*Los Alamos National Laboratory, Los Alamos, NM 87545, USA*

<sup>2</sup>*Laboratory of Atomic and Solid State Physics, Cornell University, Ithaca, NY, USA*

A major puzzle in understanding high- $T_c$  superconductivity is the microscopic origin of the linear-in-temperature ( $T$ -linear) resistivity in the strange metal state, which persists up to very high temperatures. Implicit to existing theoretical discussions of this universal ‘Planckian’ relaxation rate is the assumption that it must also be independent of doping,  $p$ . Applied to the cuprates, however, this apparently contradicts the observed strong doping-dependence ( $\propto 1/p$ ) of the slope of the  $T$ -linear resistivity over a wide doping range. Here, we show through a combination of measurements, including optical conductivity and entropy, that the plasma frequency squared  $\omega_p^2$  scales as  $p$  over a similar doping range. Together, these dependences provide compelling evidence that the relaxation rate  $1/\tau$  is indeed doping-independent (i.e. universal) throughout the entire strange metal state. Furthermore, we argue that the entire doping dependence of  $\omega_p^2$  can be understood to arise from an effective mass enhancement of a specific form proposed by Anderson [*Science* **235**, 1196 (1987)] in the context of doped Mott insulators. Such a mass enhancement originates from strong short-range repulsive interactions, while the Planckian relaxation rate itself appears to be an emergent phenomenon of independent physical origin.

The discovery of high-temperature superconductivity [1] in the cuprates was significant not only because of their atypically high superconducting transition temperatures,  $T_c$ , but also because their normal states were one of the first unconventional metals [2, 3]. This new state [4] was termed a ‘strange metal’ [5] to distinguish it from conventional metals that are well understood within Fermi liquid phenomenology [6]. Of particular interest is the electrical resistivity of this state, as it unambiguously defies Fermi liquid phenomenology [7]. Since the discovery of the strange metal state in the cuprates, similar behavior has been reported in a broad variety of materials [8–11], the majority of which also exhibit unconventional superconductivity. Today, the research of strange metals is closely tied to the search for unconventional superconductivity.

Strange metal behavior [2, 5, 10, 12, 13] in the cuprates is characterized by a linear-in-temperature ( $T$ -linear) resistivity [3, 14, 15], expressed as  $\rho = AT$ , that persists up to temperatures of approximately  $T \sim 1000$  K—limited only by chemical stability of these compounds. This form of resistivity is ‘scale-invariant’ because the only energy scale governing electrical transport is the externally imposed temperature,  $k_B T$ , rather than an intrinsic energy scale [16, 17]. This stands in stark contrast to conventional metals, whose transport behavior depends on the Fermi energy—an intrinsic property of the electronic system—together with temperature [6, 7].

While the microscopic origin of strange metal behavior remains heavily debated [2, 3, 9, 10, 12, 18–20], its  $T$ -linear resistivity reflects the near equivalence of two energy scales: the relaxation rate,  $\hbar/\tau$ , and the thermal

energy,  $k_B T$ . Hence,

$$\hbar/\tau = \alpha k_B T. \quad (1)$$

This near equivalency ( $\alpha \sim 1$ ) has been termed ‘Planckian’ due to a purported connection between energy scales arising naturally within specific theoretical frameworks [2, 4, 9, 10, 12, 19, 21, 22]. Implicit to these theoretical frameworks is a doping independence of  $\alpha$ .

In fact, values of  $\alpha$  close to unity have been reported on the basis of low-temperature resistivity measurements at select dopings in several cuprate families [23], including  $p = 0.26$  in  $\text{La}_{2-x}\text{Sr}_x\text{CuO}_4$  (LSCO). It is implied by this experimental work that similar values of  $\alpha$  must apply over a broad doping range. Because the slope  $A(p)$  of the  $T$ -linear electrical resistivity in the strange metal state is strongly doping-dependent [15, 24–28], it is not at all clear how such a purported doping-independence of  $\alpha$  can be reconciled with the observed transport behavior throughout the entire phase diagram. Such reconciliation is the subject of the present work.

## RESULTS

**Evidence for universality of the Planckian relaxation rate.** Figure 1A shows the phase diagram of LSCO indicating the strange metal state above a crossover temperature  $T_{co}(p)$ . Figure 1B shows the inverse slope,  $1/A(p)$ , of the  $T$ -linear resistivity obtained by linear regression of  $\rho(T)$  at high temperatures in LSCO over a broad range of dopings [15, 28, 30] (see *Appendix* and *Appendix*, Fig. 6).

While the strange metal state extends down to low temperatures at the ‘critical doping’  $p^* \sim 0.2$  [3, 15, 31, 32], as one moves away from  $p^*$ , the high-temperature  $T$ -linear behavior is cut off below  $T_{co}(p)$  [30], (Fig. 1). Below this temperature, the resistivity is no longer purely

---

\* email: [arkadyshekhter@gmail.com](mailto:arkadyshekhter@gmail.com)

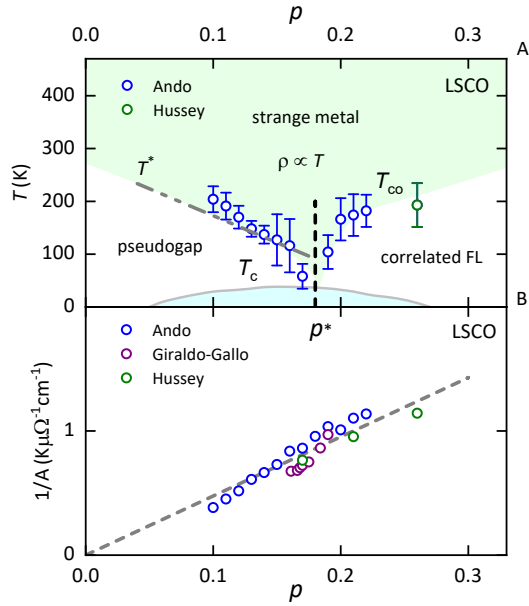


FIG. 1. Electrical resistivity in the strange metal phase. (A) Strange metal phase (shaded green) where  $\rho \approx \rho_0 + AT$  [15], where  $\rho_0$  refers  $\rho$  extrapolated to  $T = 0$ .  $T_{co}$  obtained by fitting (circles) (see Appendix). For  $p \lesssim p^*$ , this coincides roughly with  $T^*$  (dashed line) from Ref. [29]. (B)  $1/A$  (circles) from Hussey *et al.* [23, 30], and Giraldo-Gallo *et al.* [28], and from performing linear regression of data from Ando *et al.* [15] (see Appendix), Fig. 6) vs.  $p$ .

$T$ -linear and is therefore no longer scale-invariant (see Appendix). In this paper, we focus on the strange metal state exhibiting scale-invariant (pure  $T$ -linear) resistivity, which is confined to the funnel-shaped region of the phase diagram above  $T_{co}(p)$ .

Remarkably, in the strange metal state  $A(p)$  closely follows a  $1/p$  scaling over nearly a factor three doping range ( $0.1 \leq p \leq 0.26$  in Fig. 1B). This behavior can be analyzed by invoking the Einstein relation  $\sigma = e^2 \kappa D$  [7, 33], which expresses the conductivity  $\sigma = 1/\rho$  as the product of the charge compressibility  $e^2 \kappa$  and the diffusion coefficient  $D = v_F^2 \tau / 2$  at the Fermi surface, where  $v_F$  is the Fermi velocity. In Fermi liquid theory, the charge compressibility is given by  $e^2 \kappa = (1 + F_0)^{-1} e^2 \nu$  [6], where the electronic density of states on the Fermi surface,  $\nu$ , is determined by the quasiparticle effective mass  $m^*$ , as defined by the specific heat [6, 34, 35]. Here,  $(1 + F_0)^{-1}$  is the zeroth harmonic Landau interaction parameter in the charge channel. Within this framework, the resistivity takes the form  $\rho = (4\pi/\omega_p^2) \times (1/\tau)$ , where the plasma frequency squared is  $\omega_p^2 = (4\pi/2) e^2 \kappa v_F^2$ .

For an approximately parabolic band,  $\omega_p^2 = 4\pi e^2 (n/m^*) \times (1 + F_0)^{-1}$ , where  $n$  is the carrier density [36]. The Fermi-liquid factor  $(1 + F_0)^{-1}$  also appears in the observed relaxation rate  $1/\tau = (1/\tau_0) \times (1 + F_0)^{-1}$ , where  $1/\tau_0$  is the relaxation rate in the absence of Fermi-liquid effects. In the zero frequency limit of the conduc-

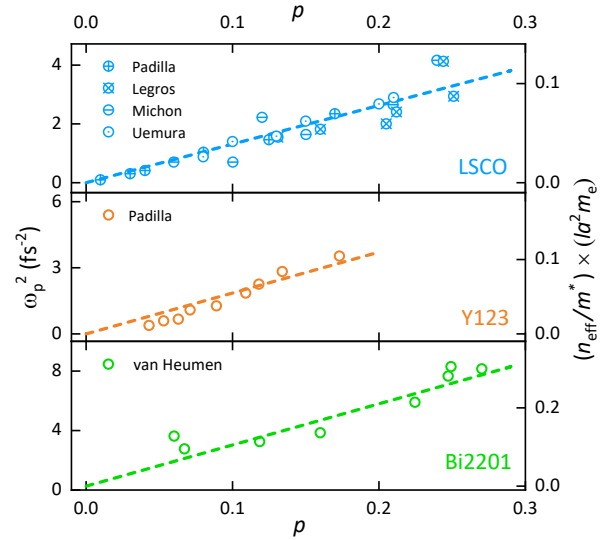


FIG. 2. Optical conductivity measurements. Inferred  $\omega_p^2$  and  $n_{\text{eff}}/m^*$  vs.  $p$  for LSCO from Padilla *et al.* [39], Legros *et al.* [40], and Michon *et al.* [41], for Y123 from Padilla *et al.* [39] using  $p$  determined by Liang *et al.* [42], and for Bi2201 from van Heumen *et al.* [43]. For LSCO, we have included estimates of  $\omega_p^2$  inferred from penetration depth measurements from Uemura *et al.* [44, 45], which lie on the same line.

tivity, it is well known that these Fermi liquid factors cancel out [33]. Despite this cancellation, both the observed  $\omega_p^2$  and  $1/\tau$  contain these factors explicitly, which will need to be taken into consideration when comparing the optical conductivity and thermodynamic measurements.

The parabolic band approximation for  $\omega_p^2$  breaks down in the cuprates over a broad doping range straddling a Van Hove singularity [37]. To retain a Drude-like representation for the plasma frequency over such a broad doping range, it is customary to introduce an effective carrier density  $n_{\text{eff}}$  [38], such that  $\omega_p^2 = 4\pi e^2 (n_{\text{eff}}/m^*) \times (1 + F_0)^{-1}$ . The deviation of  $n_{\text{eff}}$  from the actual carrier density  $n$  is expected to be most pronounced near the Van Hove singularity.

Using Eq. 1, the slope  $A(p)$  of the  $T$ -linear resistivity can be expressed as

$$A(p) = \left( \frac{4\pi}{\omega_p^2} \right) \left( \frac{k_B}{\hbar} \right) \times \alpha. \quad (2)$$

For  $\alpha$  to be doping-independent (i.e., universal), the entire doping dependence of  $A(p)$  must arise from  $\omega_p^2 \propto p$ . The two distinct possibilities,  $n_{\text{eff}}(p) \propto p$  and  $m^*(p) \propto 1/p$ , will be discussed later.

A doping dependence of  $\omega_p^2$  is readily observed in optical conductivity measurements [46]. In contrast to zero-frequency transport measurements, which depend only on the product  $\omega_p^2 \times \tau$ , optical conductivity measurements enable  $\omega_p^2$  to be separated from  $1/\tau$  by integrating the Drude peak over a frequency range comparable to its width [46]. In such measurements, the relaxation rate

acquires the complex form:  $\tau \rightarrow \tau/(1 - i\omega\tau)$ , where  $\omega$  is the frequency, and  $\tau$  is itself also generally found to be temperature- and frequency-dependent [43, 46, 47].

Figure 2 shows the plasma frequency squared in LSCO [39],  $\text{YBa}_2\text{Cu}_3\text{O}_{6+x}$  (Y123) [39], and  $\text{Bi}_{2-x}\text{Pb}_x\text{Sr}_{2-y}\text{La}_y\text{CuO}_{6+\delta}$  (Bi2201) [43]. While the slopes differ somewhat—possibly reflecting variations in electronic structure—all three systems exhibit  $\omega_p^2 \propto p$  behavior up to  $p \approx 0.3$ .

**Thermodynamic evidence for  $\omega_p^2 \propto p$  extending to high dopings.** Thermodynamic measurements [48] (Fig. 3), which predate the optical studies, provide independent evidence for  $\omega_p^2 \propto p$  scaling extending over an even broader range of dopings (up to  $p = 0.45$ ). With increasing doping ( $p \geq 0.23$ ) [48, 49], the high temperature entropy  $S(T)$  becomes increasingly linear in temperature (Fig. 3A), allowing the effective mass to be estimated directly from the electronic specific heat coefficient via  $\gamma = \partial S(T)/\partial T \approx S/T$ , using the conversion

$$\gamma = m^* \left( \frac{\pi k_B^2 N_A a^2}{3\hbar^2} \right) \approx \frac{m^*}{m_e} \times (1.4 \text{ J mol}^{-1}\text{K}^{-2}) \quad (3)$$

(where  $m_e$  is the free electron mass) valid for a quasi-two-dimensional metal [50]. Figure 3B shows that  $\gamma \approx S(T)/T$  at  $T = 300 \text{ K}$  and the inferred  $m^*$  scale as  $1/p$  for dopings  $0.23 \leq p \leq 0.45$ , spanning nearly a factor of two in doping. Figure 3C shows the entropy calculated using a tight-binding approximation of a ‘Mott band,’ in which the electronic dispersion of the bare band is reduced by a Mott enhancement factor  $m^*/m$  (see Appendix). Comparing this calculation with the data in Fig. 3A enables  $m^*/m$  to be obtained (plotted in Fig. 3D; see also Appendix and Appendix, Figs. 7 & 8).

Both the approximate estimate  $T/S_{300\text{K}}$  in Fig. 3C and the Mott-enhanced mass in Fig. 3D are found to scale as

$$\frac{m^*}{m} \approx \frac{1}{p}. \quad (4)$$

Equation 4 enables other thermodynamic quantities to be estimated from the tight-binding approximation of a Mott band, such as the plasma frequency.

Figure 4A (purple line) shows the plasma frequency squared,  $\omega_{p,\text{Mott}}^2$ , thus calculated. The purple dashed line shows the asymptotic slope of  $\omega_{p,\text{Mott}}^2$  as  $p \rightarrow 0$ , while the grey dashed line represents the experimentally observed  $p$ -linear slope of  $\omega_p^2$  in LSCO, as extracted from optical conductivity data in Fig. 2 (replotted in Fig. 4B). A clear difference in slope is visible, which persists over the entire doping range, well above  $p^*$ . Such a difference in slope is anticipated because the estimate  $\omega_{p,\text{Mott}}^2$ , derived from the entropy-informed tight-binding model, uses the density of states from specific heat measurements rather than the charge compressibility,  $e^2\kappa$ . These differ by a Fermi liquid factor; i.e.,  $e^2\kappa = (1 + F_0)^{-1} e^2\nu$  [6, 34, 35]. Since the entropy-informed  $\omega_{p,\text{Mott}}^2$  does not include the  $(1 + F_0)^{-1}$  factor, we expect the ratio  $\omega_p^2/\omega_{p,\text{Mott}}^2 = (1 + F_0)^{-1}$ . We therefore estimate  $(1 + F_0)^{-1} \approx 0.6$ ,

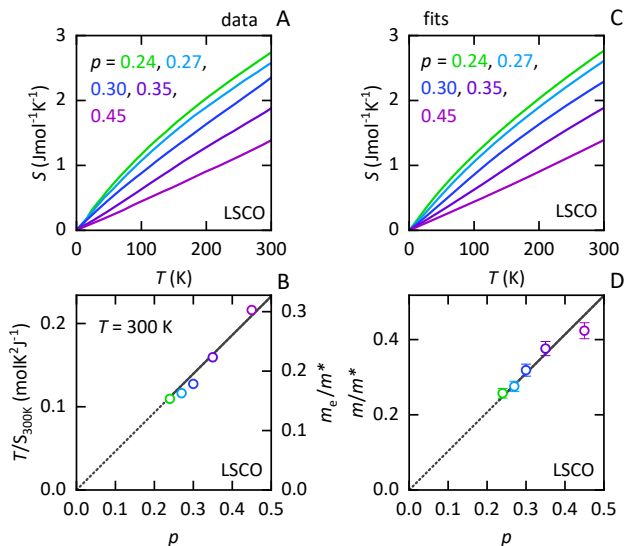


FIG. 3. Entropy measurements. (A) Measured  $S$  vs.  $T$  of LSCO at several  $p$  [49]. (B)  $T/S_{300\text{K}}$  vs.  $p$  (lines rescaled from (D)). (C) Calculated  $S$  vs.  $T$  using  $m/m^*$  from (D) (see Appendix). (D) Fitted  $m/m^*$  vs.  $p$ , where  $m$  is the band mass. The solid line corresponds to  $m/m^* = (1.03 \pm 0.02) \times p$ . The dotted line is an extrapolation.

suggesting a modest Fermi liquid renormalization of the compressibility across the entire doping range studied.

In Fig. 4B, we proceed to estimate  $\omega_p^2$  directly from the entropy data shown in Fig. 3C, using the approximate relation  $\omega_p^2/4\pi e^2 \approx (n_{\text{eff}}/m^*) \times (1 + F_0)^{-1}$ , with  $n_{\text{eff}} \approx 1/(la^2)$ . The choice of  $n_{\text{eff}}$  reflects the fact that the effective carrier density differs from the nominal carrier density  $n$  over a broad doping range, particularly near the middle of the band close to the Van Hove singularity [37]. The distinction between  $n_{\text{eff}}$  and  $n$  is evident in the behavior of a bare tight-binding band, where the corresponding plasma frequency  $\omega_{p,\text{bare}}^2$  (grey curve in Fig. 4A) evolves smoothly with doping, rather than linearly (see Appendix).

It is important to note that while  $\omega_{p,\text{Mott}}^2$  remains linear in  $p$  up to  $p \sim 0.3$  (Fig. 4A & B), it begins to bend downward on approaching the band extremity at  $p = 1$  (Fig. 4A), as expected due to the vanishing electron density in this limit. This behavior was recently highlighted in an analysis of the superfluid density in doped Mott insulators [51, 52]. The slight asymmetry in Fig. 4A is the result of us using tight-binding parameters specific to LSCO [37].

Since the  $1/A(p) \propto p$  data in Fig. 1A extend only up to  $p = 0.26$ , where  $\omega_p^2(p)$  is well approximated by a linear function, we can use Eq. 2 to obtain  $\alpha \approx 2.6$ , corresponding to the median value indicated by the horizontal dashed line in Fig. 4C. This value is similar to that estimated in Refs. [53, 54]. Taken together, the optical conductivity, penetration depth, entropy measurements, and  $T$ -linear resistivity in the strange metal state estab-

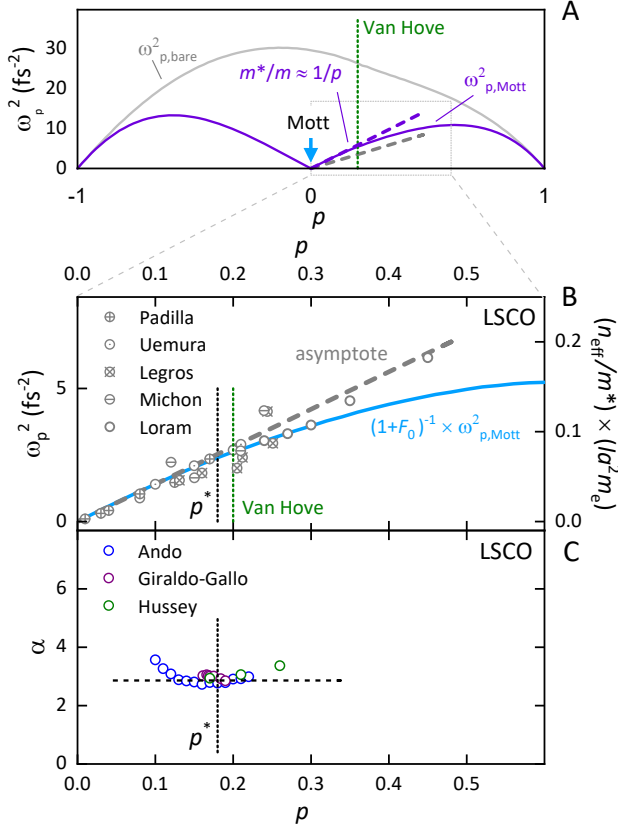


FIG. 4.  $\omega_p^2$  and  $\alpha$  in LSCO. (A) Calculated plasma frequency,  $\omega_{p,\text{bare}}^2$ , for bare band (grey curve) using tight-binding parameters from Horio *et al.* [37] (Appendix). The purple curve represents the plasma frequency,  $\omega_{p,\text{Mott}}^2$ , calculated for a tight-binding approximation for a Mott band, renormalized by  $m^*/m$  given by Eq. 4. Such behavior in a doped Mott insulator was recently discussed in Refs. [51, 52]. The purple dashed line is its  $p \rightarrow 0$  asymptote. The grey dashed line represents the data from panel B. Ratio of the dotted line slopes yields  $(1+F_0)^{-1} \approx 0.6$ . (B),  $\omega_p^2$  (and  $n_{\text{eff}}/m^*$ , right-hand axis) in LSCO from the measured optical conductivity of Padilla *et al.* [39], time-resolved THz spectroscopy of Legros *et al.* [40], and penetration depth of Uemura *et al.* [44, 45]. We also show crude estimate of  $\omega_p^2$  directly from entropy of Loram *et al.* [48, 49], using  $n_{\text{eff}}/m^* \times (la^2 m_e) \times (1+F_0)^{-1} \approx 1.4 \times (T/S) \times (1+F_0)^{-1}$  (the factor of 1.4 is from Eq. 3). The blue curve is  $\omega_{p,\text{Mott}}^2$  from panel A scaled by  $(1+F_0)^{-1}$ . (C) Values of  $\alpha$  determined using the data in Fig. 1A, Eq. 2, and the  $n_{\text{eff}}/m^* \times (1+F_0)^{-1} = 0.42 \times p/(la^2 m_e)$  asymptote from panel B.

lish the doping-independence of  $\alpha$ —i.e., universality of the Planckian relaxation rate  $1/\tau$  over the entire doping range analyzed.

**Mott physics as the mechanism for  $\omega_p^2 \propto p$ .** Given that there is no ambiguity regarding the large size (i.e.,  $n_{\text{eff}} \approx 1/la^2$ ) of the Fermi surface at  $p > 0.23$  [55–57], it is clear that  $\omega_p^2(p)$  must be driven by  $m^*/m \approx 1/p$  at higher dopings. Furthermore, the absence of a discontinuity

in the observed  $\omega_p^2(p)$  across  $p^*$  strongly suggests that  $m^*/m \approx 1/p$  continues to hold for  $p < p^*$ .

It is reassuring to note that a similar effective mass behavior to that observed at high dopings in LSCO was previously identified in  $^3\text{He}$  [34, 58]. While it was initially believed that the pressure-dependent quasiparticle mass and Landau parameters in  $^3\text{He}$  were due to its proximity to a Stoner instability [59], it was subsequently shown that such an instability could not simultaneously account for the observed magnitude of the effective mass, compressibility, and magnetic susceptibility [60–62]. Specifically, it was shown that Fermi liquid relations require the observed thermodynamic properties to be determined by an enhancement of the quasiparticle effective mass that occurs *independently* of Fermi liquid physics.

The transformative idea that enabled a quantitative understanding of the pressure-dependent Fermi liquid parameters in  $^3\text{He}$  is that the enhancement of the quasiparticle effective mass is caused by the suppression of the mobility of  $^3\text{He}$  atoms by hard-core repulsive interactions. This is referred to as an ‘almost-localized Fermi liquid,’ in analogy with a Mott insulator doped away from half-filling by a small amount  $p$  [60–62].

To account for the strong hard-core repulsion between atoms in  $^3\text{He}$ , Anderson and Vollhardt [60–62] introduced the ‘lattice-gas model’ with an on-site repulsion energy parameter  $U$ . A key feature of this model is that the number of sites differs from the number of atoms [63]. Consequently, the liquid is described by a new thermodynamic parameter  $p$  ( $\delta$  in Refs. [61, 62]), akin to an order parameter without symmetry breaking [64], which exists alongside pressure and temperature. This parameter defines a small difference between the volume per site of the lattice,  $v_s$ , and the volume per atom,  $v_a$ , expressed as  $p = 1 - v_s/v_a$ ; essentially, it acts as an effective doping. Similar to the Landau description of phase transitions [65],  $p$  itself is determined by a minimum in the free energy. While the Mott-insulating state occurs at  $p = 0$ , it is preempted in  $^3\text{He}$  by solidification at  $p \approx 0.05$ , corresponding to a pressure of 34.36 bar [62, 64].

In the limit of strong hard-core repulsion, the effective mass enhancement in  $^3\text{He}$  is inversely proportional to the doping:  $m^*/m \approx 1/2p$  [61, 62], where  $m$  is the band mass. Accordingly, the  $1/p$ -enhancement of the effective mass driven by hard-core repulsion at short distances is the hallmark of Mott physics. The comprehensive understanding of the effective mass enhancement in  $^3\text{He}$  [60–62] was predicated on the fact that the band mass  $m$  is equivalent to the free atomic mass of  $^3\text{He}$ . In the cuprates, by contrast, properly discussing the ratio  $m^*/m$  requires consideration of the fact that  $m$  refers to a band mass [66–68] that may itself be weakly doping-dependent. This was already accounted for by our use of a tight-binding approximation [37] to the Mott band.

The mass enhancement inferred from the observed entropy behavior, Eq. 4, is therefore also a hallmark of Mott physics, as originally emphasized by Vollhardt in the context of liquid  $^3\text{He}$  [61]. The approximately twofold larger

enhancement factor in LSCO, as expressed by Eq. 4, was in fact anticipated by Anderson, who extended his analysis of  $^3\text{He}$  to the cuprates using a modified argument [69, 70]. Within this physical picture, the empirical relationship  $\omega_p^2 \propto p$  observed in the cuprates must be governed predominantly by high-energy (short-range, local) repulsive interactions—closely analogous to those found in  $^3\text{He}$  [69, 71, 72].

We emphasize that the effective mass determined by the underlying Mott physics is not subject to *any* Fermi liquid renormalizations. It corresponds directly to the mass inferred from specific heat measurements. In contrast, other observables such as the compressibility and magnetic susceptibility, which are proportional to  $m^*$ , carry additional Fermi liquid renormalization factors. Understanding  $m^*$  quantitatively and independently of these factors was the original motivation in Refs. [61, 62]. The same reasoning must therefore apply when analyzing Fermi liquid factors in the cuprates.

**At low dopings, is it  $n_{\text{eff}}(p)$  or  $m^*(p)$ ?** Our conclusion above—that the doping dependence of  $\omega_p^2$  primarily reflects the doping-dependence of  $m^*(p)$  rather than  $n_{\text{eff}}(p)$ —is not, however, the prevailing view. This has to do with interpretations of the Hall coefficient  $R_H$  as direct evidence for the actual electron density  $n = 1/eR_H$  [39, 43, 55–57].

It is crucial, here, to distinguish the behavior of  $R_H$  at low temperatures in the pseudogap regime ( $T \ll T^*$ ), from that at higher temperatures. At very low dopings ( $p \lesssim 0.1$ ), Hall measurements appear to be consistent with a doping-dependent carrier density,  $n \propto p$  [57] (see *Appendix*, Fig. 9), an interpretation frequently adopted in optical conductivity studies [39, 47]. Such an interpretation implies small sections of reconstructed Fermi surface [55], including antiferromagnetism and exotic scenarios such as ‘Fermi arcs’ [57]. For  $p \gtrsim 0.1$  (the focus of the present analysis), however, the Hall coefficient shows pronounced doping-, temperature-, and magnetic field-dependences [2, 55, 57, 73, 74] (see *Appendix*, Fig. 10). As yet there is no established Fermi surface reconstruction scenario for  $p > 0.1$  that can explain such anomalous behavior at the same time as being consistent with other measurements. In particular, a reconstructed Fermi surface typically implies a phase transition with a clear discontinuity in  $R_H$  [75], a feature generally not observed experimentally [56, 57, 74].

Although  $R_H$  trends toward a value roughly consistent with one hole per planar Cu atom at very high temperatures [74] and  $p > 0.1$  (see *Appendix*, Fig. 10), several factors challenge a direct estimate of  $n_{\text{eff}}$  from  $R_H$ . These include the relatively low Fermi temperature  $T_F$  at low dopings—estimated as  $T_F \approx \pi \hbar^2 l(\omega_p^2/4\pi e^2)/k_B \sim 1000$  K at  $p = 0.1$ —and the recently reported anisotropic, non-Planckian component of the relaxation rate [76, 77]. Furthermore, even if Hall effect measurements accurately reflect  $n$ , significant deviations from band parabolicity (such as at the Van Hove singularity at  $p = 0.20$  [37]) are well understood to imply that  $n_{\text{eff}} \neq n$ .

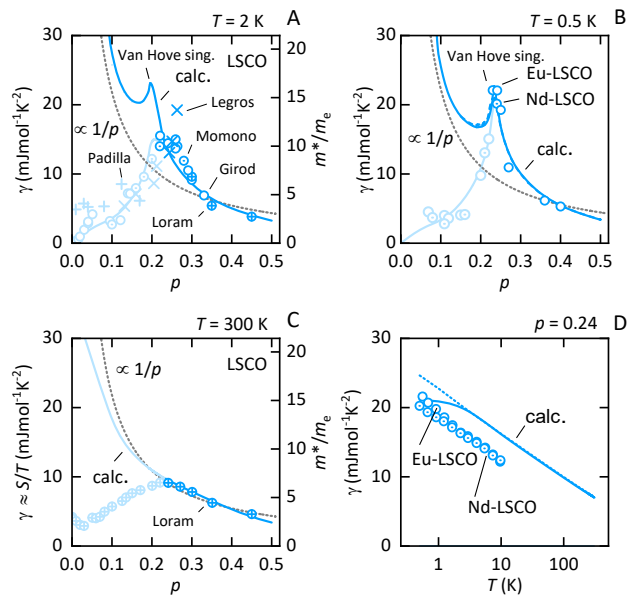


FIG. 5. Low-temperature specific heat. (A)  $\gamma$  vs.  $p$  from Refs. [48, 78, 79] and  $m^*$  vs.  $p$  from Refs. [39, 40]. The solid line shows calculations of  $\gamma = \partial S/\partial T$  (lines) at  $T = 2$  K (the lowest  $T$  accessed for  $\gamma$  measurements [79]) using  $m/m^* = 1.03 \times p$  and  $t_z/t$  of 0.07 [37] (*Appendix*). Points in the pseudogap regime ( $p \lesssim 0.23$ ) are shaded lighter for clarity. The light blue line is a guide to the eye and corresponds to  $\gamma \times n_{\text{pg}}(a^2)$ , where  $n_{\text{pg}}$  is from *Appendix SI*, Fig. 9. The dotted grey is illustrative only. (B) Measured  $\gamma$  for Nd-LSCO and Eu-LSCO [29]. Lines are calculated the same as in (A), having adjusted  $t'/t$  (see *Appendix*). (C) Measured  $\gamma \approx S/T$  of LSCO at 300 K compared with a calculation. (D) Measured  $\gamma$  versus  $T$  of Nd-LSCO and Eu-LSCO on a semilogarithmic scale at  $p = 0.24$  compared against calculated curves, using  $t_z/t$  of 0.07 (solid line), and  $t_z/t$  of 0 (dotted line) (see *Appendix*).

Time-domain terahertz spectroscopy measurements in a strong magnetic field can in principle infer the value of  $n_{\text{eff}}$  from independent measured values of the plasma frequency and the cyclotron shift. Interestingly, the mass inferred from the low-temperature cyclotron shift in the underdoped cuprates [40] is similar to that obtained from specific heat measurements (see Fig. 5), both of which are strongly suppressed at low temperatures by the pseudogap (e.g. light-shaded points in Figs. 5A). As a result, the time-domain terahertz spectroscopy estimate of  $n_{\text{eff}}$  at low temperatures is reduced by pseudogap effects and therefore does not reflect its value in the strange metal state above  $T^*$ . The significant discrepancy [40] between  $n_{\text{eff}}$  and  $n$  inferred from  $R_H$  suggests that the electrical conductivity within the pseudogap state is also not well accounted for by the Drude model.

To avoid the pseudogap-driven suppression of  $n_{\text{eff}}$ , one must turn to measurements above  $T^*$  [3]. Indeed, photoemission experiments for  $p \lesssim p^*$  typically report that the full cuprate Fermi surface re-emerges at temperatures above  $T^*$  [80], implying a carrier density on the order of

one hole per planar Cu site. Given this observation, together with the absence of a direct relationship between  $n_{\text{eff}}$  and  $R_{\text{H}}$ , there is no conclusive evidence that the Fermi surface volume significantly deviates from one hole per Cu in the strange metal state at  $T > T^*$ .

**Effect of the pseudogap on  $\omega_{\text{p}}^2$ .** Although there are no direct measurements of  $n_{\text{eff}}(p)$  and  $m^*(p)$  in the strange metal state above  $T^*$  at  $p < p^*$ , experimental evidence suggests that the plasma frequency is largely unaffected by the pseudogap. This conclusion is supported by: (i) the absence of a discernible jump in  $\omega_{\text{p}}^2$  across  $p^*$  in Fig. 4B; (ii) the weak temperature dependence of  $\omega_{\text{p}}^2$  observed in optical conductivity measurements on Bi2201 [43] and Bi<sub>2</sub>Sr<sub>2</sub>Ca<sub>0.92</sub>Y<sub>0.08</sub>Cu<sub>2</sub>O<sub>8- $\delta$</sub>  (Bi2212) [19, 81]; and (iii) the tight-binding calculation (see *Appendix*) that quantitatively reproduces (with proper use of the Fermi liquid compressibility renormalization factor) the values of  $\omega_{\text{p}}^2$  in optical conductivity, THz spectroscopy, and penetration depth measurements shown in Fig. 4B (purple line) using Eq. 4, without introducing any additional parameters—in particular, without accounting for the pseudogap.

One way to understand the weak effect of the pseudogap on  $\omega_{\text{p}}^2$ , phenomenologically, is through the redistribution of electronic states upon the opening of the pseudogap. If the redistributed states remain largely within the Drude peak, the inferred value of  $\omega_{\text{p}}^2$  will not change significantly [46].

**Is there a quantum critical mass enhancement in the cuprates?** Several recent studies have reported a strong quantum-critical mass enhancement near  $p^*$  [29, 79, 82] (see, e.g., Fig. 5). It is important to note that such an enhancement would only challenge the observed relation  $\omega_{\text{p}}^2 \propto p$  (Figs. 2 and 4B) if  $n_{\text{eff}}$  were interpreted literally as the carrier density  $n$ . Consequently, such an enhancement near  $p^*$  does not in itself challenge the universality of the Planckian relaxation rate (Fig. 4C). As with the effects of the pseudogap, quantum criticality would only have a significant impact on  $\omega_{\text{p}}^2$  if it redistributed spectral weight over a sufficiently wide energy range. A quantum-critical mass enhancement *does*, however, challenge thermodynamic measurements pertaining to  $m^*/m \approx 1/p$ , thereby warranting careful scrutiny. Since quantum oscillation results [82] have already been discussed in some detail elsewhere [83], here we focus only on the low-temperature thermodynamic data [29, 48, 78, 79] for  $p > 0.23$ , where the pseudogap no longer affects  $\gamma$  (see *Appendix*, Fig. 11).

Figures 5A & B show the doping dependence of the low-temperature electronic specific heat coefficient  $\gamma$  in LSCO [78, 79], and in La<sub>2- $y$ - $x$</sub> Nd <sub>$y$</sub> Sr <sub>$x$</sub> CuO<sub>4</sub> (Nd-LSCO) and La<sub>2- $y$ - $x$</sub> Eu <sub>$y$</sub> Sr <sub>$x$</sub> CuO<sub>4</sub> (Eu-LSCO) [29], respectively. We also complement the  $\gamma$  measurements in LSCO with cyclotron mass measurements [40]. The sharp peak in the low-temperature specific heat coefficient at  $p \sim 0.2$  has been interpreted as evidence of mass enhancement near a quantum critical point [29, 79]. A quantum critical origin of this mass enhancement was further made plausible in

this work by the observation of a logarithmic temperature dependence of the electronic specific heat coefficient (see Fig. 5D) [29].

Interestingly, the same tight-binding approximation of a Mott band that captures the doping- and temperature-dependent entropy behavior observed up to room temperature in Fig. 3 reproduces the low-temperature behavior in Figs. 5A & B without any additional adjustable parameters. This suggests that the observed low-temperature peak is a direct consequence of non-parabolic band effects—specifically the Van Hove singularity—rather than quantum-critical mass enhancement. It is reassuring that the same calculation also accurately captures the ( $T = 300$  K) high temperature behavior of  $\gamma \approx S/T$ , where the effects of the Van Hove singularity can no longer be seen (see Fig. 5C), and the logarithmic temperature dependence shown in Fig. 5D [29] (see *Appendix*).

We conclude that in all three systems, the peak in  $\gamma$  around  $p = 0.2$  is a result of the Van Hove singularity effectively riding on top of a smoothly varying  $p$ -inverse background [61, 62] (grey curve). This is evident on contrasting the low-temperature behavior (Figs. 5A and B) with the high-temperature behavior (Fig. 5C). As the temperature is increased, the Van Hove effects weaken, and we are left only with the  $p$ -inverse background (as directly evident in Fig. 5C). The strong decrease in  $\gamma$  with increasing  $p$  cannot be accounted for solely by the Van Hove singularity. In the case of LSCO, the observation of a sharp Van Hove peak is preempted by the opening of the pseudogap, which reduces  $\gamma$  (and the inferred  $m^*$ ) for  $p < 0.23$ .

As a side note, we point out that the Van Hove singularity also does not significantly affect  $\omega_{\text{p}}^2(p)$ —a detail captured by band structure calculations (purple curves in Figs. 4A & B, using the same tight-binding approximation of a Mott band employed to reproduce the entropy in Fig. 3) without any additional adjustable parameters.

Quantum-critical mass enhancement thus appears to be a weak effect in the cuprates, in much the same way as the effect of order-parameter fluctuations on mass enhancement was found to be a weak effect in liquid <sup>3</sup>He [61, 62].

## DISCUSSION

If the Mott mechanism for mass enhancement applies across the entire hole-doped regime of the cuprates, then the effective mass obeys  $m^*/m \approx 1/p$  throughout this region. Because this enhancement is not driven by Fermi liquid renormalizations,  $m^*$  represents the actual quasiparticle mass on the Fermi surface, not subject to additional Fermi liquid factors [6], as is similarly the case in liquid <sup>3</sup>He [61]. This stands in contrast to other thermodynamic observables, such as the compressibility and magnetic susceptibility, which are subject to further renormalization by Fermi liquid interaction parameters. In particular, the observed compressibility and the re-

laxation rate that enter in the Einstein relation for the conductivity [33], both carry an additional Fermi liquid renormalization factor. Therefore, the Mott-induced mass enhancement modifies  $\omega_p^2$ , but does not affect the relaxation rate  $1/\tau$ . As a result, the Mott-induced mass enhancement does not cancel out in the zero-frequency conductivity, because it has a non-Fermi liquid origin. It is only through such a mechanism that the resistivity slope  $A(p) \propto 1/p$  can exhibit a strong doping dependence, while the Planckian relaxation rate (characterized by the coefficient  $\alpha$ ) remains universal.

In a recent study [23], the Planckian relaxation rate in the cuprates was deemed universal, based on several inferred values of  $\alpha$  close to unity—consistent with theoretical conjectures [4, 19, 21]. While several different cuprate compositions were examined, the coefficient ( $\alpha \approx 0.9$ ) was determined only at  $p = 0.26$  in LSCO, using a Drude formula in which  $n = (1 - p)/la^2$  and  $m^* \approx 10m_e$ . We note that this value of  $m^*$  is somewhat higher than our estimate in the strange metal state of LSCO (compare Figs. 5A and B). The dominant source of the discrepancy between their reported  $\alpha$  value and our estimate ( $\alpha \approx 2.6$ , Fig. 4C) is the significantly smaller slope of the residual  $T$ -linear resistivity at temperatures well below the crossover temperature  $T_{co}$  indicated in Fig. 1A (see also *Supporting Information*, Text 1 and Fig. 12).

Due to  $\omega/T$  scaling, the doping-independence of the Planckian relaxation rate is expected to apply not only to the temperature dependence but also to the frequency dependence of  $1/\tau$  at high frequencies. Indeed, optical conductivity measurements indicate that the slope of the  $\omega$ -linear scattering rate,  $\tau^{-1}(\omega)$ , is also only weakly doping dependent—i.e., it too points to universality [46].

Our findings provide a novel perspective for understanding Planckian relaxation as a universal phenomenon [4, 53, 54]—not only in the cuprates over a wide doping range, but also possibly in a broader class of strange metals [4, 8–11, 19] (e.g., see *Supporting Information*, Text 2 and Fig. 13).

If the above picture of mass enhancement holds throughout the strange metal phase, it implies the coexistence of universal Planckian relaxation and Mott physics. Mott physics arises from high-energy (short-range) electronic interactions, while Planckian relaxation emerges from low-energy fluctuations. As shown in earlier studies of liquid  $^3\text{He}$  [61, 62], such a decoupling between high- and low-energy physics is not without precedent.

## APPENDIX

**Linear regression at high temperatures to determine  $A$  and  $T_{co}$ .** To establish whether the data is well described by a  $T$ -linear behavior at high temperatures in Fig. 1A, in *Appendix Fig. 6* we fit the function  $\rho = \rho_0 + AT$  to the in-plane resistivity data in LSCO [15] above 250 K for each hole doping. While this tempera-

ture is chosen arbitrarily, we find that the linear regression continues to describe the data for a range of temperatures below this value. At  $p^* = 0.18$  [57], the  $T$ -linear behavior extends all the way from 400 K down to  $T_c$ . We define the crossover temperature  $T_{co}$  as the characteristic temperature below which the resistivity deviates from linearity. We choose  $3 \mu\Omega\text{cm}$  as the threshold above which a deviation from linearity is considered significant and estimate the error in  $T_{co}$  by increasing the threshold to  $10 \mu\Omega\text{cm}$ .

The downward departure of  $1/A$  from the dashed line below  $p \approx 0.15$  in Fig. 1A could arise either from a larger effect of the pseudogap at lower dopings or from a larger crossover temperature at these dopings. It is also well-known that at these lower dopings, disorder effects are prevalent [84], leading to a glassy behavior approaching  $p \sim 0.05$ .

### Estimates of $\omega_p^2$ from entropy measurements.

While the entropy  $\omega_p^2$  estimates in Fig. 4B deviate significantly from the calculated  $\omega_p^2(p)$  curve, the full temperature and doping-dependence of the measured entropy is well reproduced (compare Figs. 3B & C) by the tight-binding calculations using  $m^*/m \approx 1/p$ .

### Tight-binding electronic dispersion used in calculations.

Throughout, we assume the tight-binding approximation for a Mott band, where the electronic dispersion is reduced by a factor  $m/m^*$  [85, 86] so that

$$\begin{aligned} \epsilon_k = \frac{m}{m^*} \Big[ & -2t(\cos(ak_x) + \cos(ak_y)) \\ & + 4t' \cos(ak_x) \cos(ak_y) - 2t''(\cos(2ak_x) + \cos(2ak_y)) \\ & + 4t'''(\cos(ak_x) \cos(2ak_y) + \cos(ak_y) \cos(2ak_x)) \\ & + 2t_z \cos(ak_x/2) \cos(ak_y/2) [\cos(ak_x) - \cos(ak_y)]^2 \\ & \times \cos(ck_z) \Big] + \mu. \end{aligned} \quad (5)$$

Here,  $k_x$ ,  $k_y$ , and  $k_z$  represent components of the reciprocal lattice vector,  $a \approx 3.8 \text{ \AA}$  is the planar lattice spacing,  $c = 2l \approx 13.2 \text{ \AA}$  is the interlayer lattice spacing, and  $\mu$  is the chemical potential, adjusted to produce an unreconstructed Fermi surface cross-section comprising  $1 + p$  holes for  $p < 0.2$  or  $1 - p$  electrons for  $p > 0.2$ , consistent with Luttinger's theorem [87, 88]. We use the nearest neighbor hopping,  $t = 430 \text{ meV}$ , as determined for the bare conduction band by electronic structure calculations [66–68], and ratios  $t'/t$ ,  $t''/t'$ , and  $t_z/t$  that are fixed. These ratios have been determined elsewhere [37]:

	$t'/t$	$t''/t'$	$t'''/t''$	$t_z/t$
LSCO	0.12	0.50	0	0.07
Nd-LSCO	0.14	0.50	0	0.07
Eu-LSCO	0.14	0.50	0	0.07

(6)

**Calculating the entropy.** The electronic density of

states per copper oxide plane is [36]

$$\rho(E) = 2la^2 \int \frac{d^3k}{(2\pi)^3} \delta(\epsilon_k - E). \quad (7)$$

Here, the prefactor of 2 corresponds to the number of spins, and  $\delta(\epsilon_k - E)$  is a delta function defined such that  $\int \rho(E)dE = 2$ . The entropy is then given by [36]:

$$S = N_A \int_{-\infty}^{\infty} dE \rho(E) [n_F \ln n_F + [1 - n_F] \ln(1 - n_F)], \quad (8)$$

where  $n_F = 1/(1 + \exp\{E/k_B T\})$  is the Fermi-Dirac distribution, and  $N_A$  is Avogadro's number.

**Procedure to determine  $m/m^*$ .** Using the above fixed values of  $t$  and the ratios  $t'/t$ ,  $t''/t'$ , and  $t_z/t$ , we calculate the entropy in Fig. 3C in the main text using Eq. 8. Agreement with the experimentally measured entropy in Fig. 3A is achieved by adjusting  $m/m^*$  in Eq. 5. The resulting values of  $m/m^*$  are plotted in Fig. 3D in the main text.

The errors (see *Appendix* Fig. 7) are estimated from the small difference  $\Delta S$  of the calculated entropy curve from the experimental curve. This shows no systematic trends, suggesting that the difference is primarily the result of random error. We assume the largest deviation of  $\Delta S$  from zero to provide an estimate of the error  $\delta S$  in  $S$ . Since the magnitude of the entropy at a given temperature scales roughly with the effective mass, we can infer an approximate error for the fitted effective mass given by  $\delta m^* = (\delta S/S)m^*$ .

**Calculating  $\omega_p^2$ .** The plasma frequency of a ‘Mott band’ is obtained using

$$\frac{\omega_{p,\text{Mott}}^2}{4\pi e^2} = 2 \int_{\text{BZ}} \frac{d^3k}{(2\pi)^3} \mathbf{v}_x^2(k) \left. \frac{\partial n_F(E, T)}{\partial E} \right|_{E=\epsilon_k}, \quad (9)$$

where  $\mathbf{v}_k = \hbar^{-1} \nabla_k \epsilon_k$  is the group velocity,  $V$  is volume, and  $\epsilon_k$  is the tight binding approximation, includ-

ing the prefactor of  $m/m^*$  given by Eq. 4. In the zero-temperature limit, this expression can be reduced to an integral over the Fermi surface area [36, 89]. The observed plasma frequency differs by a factor of  $(1 + F_0)^{-1}$  as described in the main text. For the calculation of a non-interacting bare band (Fig. 4A), we repeat the calculation by setting  $m/m^* = 1$ .

**Effect of interlayer hopping on  $\gamma$  in the vicinity of the Van Hove singularity.** At temperatures below  $\sim 2 K$ ,  $\gamma$  in Fig. 5D becomes sensitive to the interlayer hopping. Whereas Ref. [37] finds  $t_z/t = 0.07$ , Ref. [90] finds  $t_z/t = 0.03$ . The measurements of  $\gamma$  close to  $p = 0.23$  were performed under strong magnetic fields [29]. It has been argued that orbital-averaging leads to a suppression of the interlayer hopping [91], which could cause the effective ratio  $t_z/t$  to drop to a significantly smaller value. For  $t_z/t = 0$ , the logarithmic divergence in Fig. 5D continues down to  $T = 0$ .

Impurity scattering introduces a residual scattering rate at  $T = 0$ , which can also cause  $\gamma$  to saturate [29]. Angle-dependent magnetoresistance measurements have found the residual scattering rate to be momentum-dependent [92]. However, since the Fermi velocity vanishes along all momentum directions at the point of the Fermi surface where the Van Hove singularity occurs, angle-dependent magnetoresistance measurements are unable to constrain a value for this scattering rate at this point on the Fermi surface [92]. In order for the mean free path to remain non-vanishing at this point,  $\tau^{-1}$  must vanish at this point.

## ACKNOWLEDGMENTS

We thank Ross McDonald for a critical reading of the manuscript. This work was performed as part of the Department of Energy (DoE) BES project ‘Science of 100 tesla.’ The entropy calculation procedures were developed as part of an LDRD DR project at Los Alamos National Laboratory. The National High Magnetic Field Laboratory is funded by NSF Cooperative Agreements DMR-1157490 and 1164477, the State of Florida and DoE.

- 
- [1] J. G. Bednortz and K. A. Muller, *Z. Phys.* **64**, 189 (1986).
  - [2] P. W. Anderson, *Science* **256**, 1526 (1992).
  - [3] B. Keimer, S. A. Kivelson, M. R. Norman, S. Uchida, and J. Zaanen, *Nature* **518**, 179 (2015).
  - [4] J. Zaanen, *Nature* **430**, 512 (2004).
  - [5] P. W. Anderson, in *AIP Conference Proceedings*, Vol. 169 (AIP Publishing, 1988) pp. 141–157.
  - [6] L. D. Landau, *Sov. Phys. JETP* **3**, 920 (1957).
  - [7] D. Pines and P. Nozieres, *Theory Of Quantum Liquids* (CRC Press, 1999).
  - [8] J. A. N. Bruin, H. Sakai, R. S. Perry, and A. P. Mackenzie, *Science* **339**, 804 (2013).
  - [9] S. A. Hartnoll and A. P. Mackenzie, *Reviews of Modern Physics* **94** (2022), 10.1103/RevModPhys.94.041002.
  - [10] P. W. Phillips, N. E. Hussey, and P. Abbamonte, *Science* **377** (2022), 10.1126/science.abh4273.
  - [11] Y. Cao, D. Chowdhury, D. Rodan-Legrain, O. Rubies-Bigorda, K. Watanabe, T. Taniguchi, T. Senthil, and P. Jarillo-Herrero, *Phys. Rev. Lett.* **124**, 076801 (2020).
  - [12] C. M. Varma, P. B. Littlewood, S. Schmitt-Rink, E. Abrahams, and A. Ruckenstein, *Phys. Rev. Lett.* **63**, 1996 (1989).
  - [13] N. Nagaosa, *Journal of Physics and Chemistry of Solids* **53**, 1493 (1992).

- [14] S. Martin, A. T. Fiory, R. M. Fleming, L. F. Schneemeyer, and J. V. Waszczak, *Phys. Rev. B* **41**, 846 (1990).
- [15] Y. Ando, S. Komiya, K. Segawa, S. Ono, and Y. Kurita, *Phys. Rev. Lett.* **93**, 267001 (2004).
- [16] K. G. Wilson and J. Kogut, *Physics Reports* **12**, 75 (1974).
- [17] H. v. Löhneysen, A. Rosch, M. Vojta, and P. Wölfle, *Reviews of Modern Physics* **79**, 1015 (2007).
- [18] V. J. Emery and S. A. Kivelson, *Physical Review Letters* **74**, 3253 (1995).
- [19] J. Zaanen, *SciPost Phys.* **6**, 061 (2019).
- [20] C. M. Varma, *Rev. Mod. Phys.* **92**, 031001 (2020).
- [21] R. A. Davison, K. Schalm, and J. Zaanen, *Phys. Rev. B* **89**, 245116 (2014).
- [22] V. Aji and C. M. Varma, *Phys. Rev. Lett.* **99**, 067003 (2007).
- [23] A. Legros *et al.*, *Nature Phys.* **15**, 142 (2019).
- [24] H. Takagi, B. Batlogg, H. L. Kao, J. Kwo, R. J. Cava, J. J. Krajewski, and W. F. Peck, *Phys. Rev. Lett.* **69**, 2975 (1992).
- [25] T. Ito, K. Takenaka, and S. Uchida, *Phys. Rev. Lett.* **70**, 3995 (1993).
- [26] T. Watanabe, T. Fujii, and A. Matsuda, *Phys. Rev. Lett.* **79**, 2113 (1997).
- [27] N. Barišić, M. K. Chan, Y. Li, M. Greven, *et al.*, *Proceedings of the National Academy of Sciences* **110**, 12235 (2013), edited by J. C. Seamus Davis, Cornell University, Ithaca, NY.
- [28] P. Giraldo-Gallo, J. A. Galvis, Z. Stegen, K. A. Modic, F. F. Balakirev, J. B. Betts, X. Lian, C. Moir, S. C. Riggs, J. Wu, A. T. Bollinger, X. He, I. Bozovic, B. J. Ramshaw, R. D. McDonald, G. S. Boebinger, and A. Shekhter, *Science* **361**, 479 (2018).
- [29] B. Michon *et al.*, *Nature* **567**, 218 (2019).
- [30] N. Hussey, R. Cooper, X. Xu, Y. Wang, I. Mouzopoulou, B. Vignolle, and C. Proust, *Philosophical Transactions of the Royal Society A: Mathematical, Physical and Engineering Sciences* **369**, 1626 (2011).
- [31] A. P. Mackenzie, S. R. Julian, D. C. Sinclair, and C. T. Lin, *Phys. Rev. B* **53**, 5848 (1996).
- [32] R. A. Cooper, Y. Wang, B. Vignolle, O. J. Lipscombe, S. M. Hayden, Y. Tanabe, T. Adachi, Y. Koike, M. Nohara, H. Takagi, C. Proust, and N. E. Hussey, *Science* **323**, 603 (2009).
- [33] A. M. Finkel'stein, in *Soviet Scientific Reviews, Section A: Physics Reviews*, Vol. 14, Part 2, edited by I. M. Khalatnikov (CRC Press, 1990) pp. 1–101.
- [34] A. J. Leggett, *Rev. Mod. Phys.* **47**, 331 (1975).
- [35] A. J. Leggett, *Annals of Physics* **46**, 76 (1968).
- [36] N. W. Ashcroft and N. D. Mermin, *Solid State Physics* (Saunders College Publishing, Orlando, 1976).
- [37] M. Horio *et al.*, *Phys. Rev. Lett.* **121**, 077004 (2018).
- [38] D. N. Basov, R. D. Averitt, D. van der Marel, M. Dressel, and K. Haule, *Rev. Mod. Phys.* **83**, 471 (2011).
- [39] W. J. Padilla, Y. S. Lee, M. Dumm, G. Blumberg, S. Ono, K. Segawa, S. Komiya, Y. Ando, and D. N. Basov, *Phys. Rev. B* **72**, 060511 (2005).
- [40] A. Legros, K. Post, P. Chauhan, D. Rickel, X. He, X. Xu, X. Shi, I. Bozovic, S. Crooker, and N. Armitage, *Physical Review B* **106**, 195110 (2022), editors' Suggestion.
- [41] B. Michon, C. Berthod, C. W. Rischau, A. Ataei, L. Chen, S. Komiya, S. Ono, L. Taillefer, D. van der Marel, and A. Georges, *Nature Communications* **14**, Article number: 3033 (2023).
- [42] R. Liang, D. A. Bonn, and W. N. Hardy, *Phys. Rev. B* **73**, 180505 (2006).
- [43] E. van Heumen, X. Feng, S. Cassanelli, L. Neubrand, L. de Jager, M. Berben, Y. Huang, T. Kondo, T. Takeuchi, and J. Zaanen, *Physical Review B* **106**, 054515 (2022).
- [44] Y. J. Uemura, G. M. Luke, B. J. Sternlieb, J. H. Brewer, J. F. Carolan, W. N. Hardy, R. Kadono, J. R. Kempton, R. F. Kiefl, S. R. Kreitzman, P. Mulhern, T. M. Rise-man, D. L. Williams, B. X. Yang, S. Uchida, H. Takagi, J. Gopalakrishnan, A. W. Sleight, M. A. Subramanian, C. L. Chien, M. Z. Cieplak, G. Xiao, V. Y. Lee, B. W. Statt, C. E. Stronach, W. J. Kossler, and X. H. Yu, *Phys. Rev. Lett.* **62**, 2317 (1989).
- [45] Y. J. Uemura, L. P. Le, G. M. Luke, B. J. Sternlieb, W. D. Wu, J. H. Brewer, T. M. Riseman, C. L. Seaman, M. B. Maple, M. Ishikawa, D. G. Hinks, J. D. Jorgensen, G. Saito, and H. Yamochi, *Physical Review Letters* **66**, 2665 (1991).
- [46] D. N. Basov and T. Timusk, *Reviews of Modern Physics* **77**, 721 (2005).
- [47] B. Michon, A. B. Kuzmenko, M. K. Tran, B. McElfresh, S. Komiya, S. Ono, S. Uchida, and D. van der Marel, *Physical Review Research* **3**, 043125 (2021).
- [48] J. W. Loram *et al.*, *J. Physics and Chemistry of Solids* **62**, 59 (2001).
- [49] J. L. Tallon and J. G. Storey, *Frontiers in Physics* **10**, 1030616 (2022).
- [50] P. M. C. Rourke, A. F. Bangura, T. M. Benseman, M. Matusiak, J. R. Cooper, A. Carrington, and N. E. Hussey, *New J. Phys.* **12**, 105009 (2010).
- [51] P. W. Phillips, L. Yeo, and E. W. Huang, *Nature Physics* **16**, 1175 (2020).
- [52] J. Zaanen, *Nature Physics* **16**, 1171 (2020).
- [53] A. Shekhter, M. K. Chan, R. D. McDonald, and N. Harrison, *arXiv preprint arXiv:2504.02179* (2025).
- [54] C. C. Homes, S. V. Dordevic, M. Strongin, D. A. Bonn, R. Liang, W. N. Hardy, S. Komiya, Y. Ando, G. Yu, N. Kaneko, X. Zhao, M. Greven, D. N. Basov, and T. Timusk, *Nature* **430**, 539 (2004).
- [55] S. Badoux, W. Tabis, F. Laliberte, G. Grissonnanche, B. Vignolle, D. Vignolles, J. Beard, D. A. Bonn, W. N. Hardy, R. Liang, N. Doiron-Leyraud, L. Taillefer, and C. Proust, *Nature* **531**, 210 (2016).
- [56] C. Putzke, S. Benhabib, W. Tabis, J. Ayres, Z. Wang, L. Malone, S. Licciardello, J. Lu, T. Kondo, T. Takeuchi, N. E. Hussey, J. R. Cooper, and A. Carrington, *Nature Physics* **17**, 826 (2021).
- [57] Y. Ando, Y. Kurita, S. Komiya, S. Ono, and K. Segawa, *Phys. Rev. Lett.* **92**, 197001 (2004).
- [58] J. C. Wheatley, *Rev. Mod. Phys.* **47**, 415 (1975).
- [59] S. Doniach and S. Engelsberg, *Phys. Rev. Lett.* **17**, 750 (1966).
- [60] P. W. Anderson and W. F. Brinkman, *The Helium Liquids: Proceedings of the Fifteenth Scottish Universities Summer School in Physics, 1974*, edited by J. Armitage and I. Farquhar, NATO Advanced Study Institutes (Academic Press, 1975).
- [61] D. Vollhardt, *Rev. Mod. Phys.* **56**, 99 (1984).
- [62] D. Vollhardt, P. Wolfe, and P. W. Anderson, *Phys. Rev. B* **35**, 6703 (1987).
- [63] A. F. Andreev and I. M. Lifshitz, *Soviet Physics JETP* **29**, 1107 (1969), *zh. Eksp. Teor. Fiz.* 56, 2057-2068 (June,

- 1969).
- [64] E. R. Grilly, *Journal of Low Temperature Physics* **4**, 615 (1971).
- [65] L. D. Landau and E. M. Lifshitz, *Statistical Physics, Third Edition, Part 1: Volume 5 (Course of Theoretical Physics, Volume 5)*, 3rd ed., Course of Theoretical Physics, Vol. 5 (Butterworth-Heinemann, Oxford, 1980).
- [66] L. F. Mattheiss, *Phys. Rev. Lett.* **58**, 1028 (1987).
- [67] D. J. Singh and W. E. Pickett, *Physica C* **C235-240**, 2113 (1994).
- [68] E. Pavarini, I. Dasgupta, T. Saha-Dasgupta, O. Jepsen, and O. K. Andersen, *Phys. Rev. Lett.* **87**, 047003 (2001).
- [69] P. W. Anderson, *Science* **235**, 1196 (1987).
- [70] Z. Zou and P. W. Anderson, *Physical Review B* **37**, 627 (1988).
- [71] M. Grilli and G. Kotliar, *Phys. Rev. Lett.* **64**, 1170 (1990).
- [72] P. A. Lee and N. Nagaosa, *Phys. Rev. B* **46**, 5621 (1992).
- [73] T. R. Chien, Z. Z. Wang, and N. P. Ong, *Physical Review Letters* **67**, 2088 (1991).
- [74] S. Ono, S. Komiyama, and Y. Ando, *Phys. Rev. B* **75**, 024515 (2007).
- [75] G. Grüner, *Density Waves in Solids*, Frontiers in Physics, Vol. 89 (Perseus Publishing, Reading, Massachusetts, 1994).
- [76] Y. Fang, G. Grissonnanche, A. Legros, S. Verret, F. Laliberte, C. Collignon, A. Ataei, M. Dion, J. Zhou, D. Graf, M. J. Lawler, P. A. Goddard, L. Taillefer, and B. J. Ramshaw, *Nat. Phys.* **18**, 558 (2022).
- [77] A. Ataei, A. Gourgout, G. Grissonnanche, L. Chen, J. Baglo, M.-E. Boulanger, F. Laliberte, S. Badoux, N. Doiron-Leyraud, V. Oliviero, S. Benhabib, D. Vignolles, J.-S. Zhou, S. Ono, H. Takagi, C. Proust, and L. Taillefer, *Nature Physics* **18**, 1420 (2022).
- [78] N. Momono, T. Matsuzaki, M. Oda, and M. Ido, *Journal of the Physical Society of Japan* **71**, 2832 (2002).
- [79] C. Girod, D. LeBoeuf, A. Demuer, G. Seyfarth, S. Imajo, K. Kindo, Y. Kohama, M. Lizaire, A. Legros, A. Gourgout, H. Takagi, T. Kurosawa, M. Oda, N. Momono, J. Chang, S. Ono, G.-Q. Zheng, C. Marcenat, L. Taillefer, and T. Klein, *Phys. Rev. B* **103**, 214506 (2021).
- [80] M. R. Norman, H. Ding, M. Randeria, J. C. Campuzano, T. Yokoya, T. Takeuchi, T. Takahashi, T. Mochiku, K. Kadowaki, P. Guptasarma, and D. G. Hinks, *Nature* **392**, 157 (1998).
- [81] D. van der Marel, H. J. A. Molegraaf, J. Zaanen, Z. Nussinov, F. Carbone, A. Damascelli, H. Eisaki, M. Greven, P. H. Kes, and M. Li, *Nature* **425**, 271 (2003).
- [82] B. J. Ramshaw, S. E. Sebastian, R. D. McDonald, J. Day, B. S. Tan, Z. Zhu, J. B. Betts, R. Liang, D. A. Bonn, W. N. Hardy, and N. Harrison, *Science* **348**, 317 (2015).
- [83] A. Shekhter, K. A. Modic, R. D. McDonald, and B. J. Ramshaw, *Phys. Rev. B* **95**, 121106 (2017).
- [84] F. Rullier-Albenque, H. Alloul, F. Balakirev, and C. Proust, *Europhysics Letters* **81**, 37008 (2008).
- [85] W. F. Brinkman and T. M. Rice, *Phys. Rev. B* **2**, 4302 (1970).
- [86] G. Kotliar and J. Liu, *Phys. Rev. B* **38**, 5142 (1988).
- [87] J. M. Luttinger and J. C. Ward, *Phys. Rev.* **118**, 1417 (1960).
- [88] J. M. Luttinger, *Phys. Rev.* **119**, 1153 (1960).
- [89] T. Timusk and B. Statt, *Rep. Prog. Phys.* **62**, 61 (1999).
- [90] Y. Zhong, Z. Chen, S.-D. Chen, K.-J. Xu, N. Hashimoto, Y. He, S.-K. Mo, and Z.-X. Shen, *Proc. Natl. Acad. USA* **119**, e2204630119 (2022).
- [91] S. Musser, D. Chowdhury, P. A. Lee, and T. Senthil, *Phys. Rev. B* **105**, 125105 (2022).
- [92] G. Grissonnanche, Y.-W. Fang, A. Legros, S. Verret, F. Laliberte, C. Collignon, J.-S. Zhou, D. Graf, P. A. Goddard, L. Taillefer, and B. J. Ramshaw, *Nature* **595**, 667 (2021).
- [93] J. Ayres, M. Berben, M. Culo, Y.-T. Hsu, E. van Heumen, Y. Huang, J. Zaanen, T. Kondo, T. Takeuchi, J. R. Cooper, C. Putzke, S. Friedemann, A. Carrington, and N. E. Hussey, *Nature* **595**, 661 (2021).
- [94] A. Shekhter, R. D. McDonald, L. E. Winter, Y. Wu, W. Bi, X. Lian, Z. Jiang, Y. Lai, R. J. McQueeney, J.-X. Zhu, B. J. Ramshaw, and R. E. Baumbach, arXiv preprint arXiv:2303.08930 (2023), submitted on 15 Mar 2023.
- [95] J. M. Wade, J. W. Loram, K. A. Mirza, J. R. Cooper, and J. L. Tallon, *Journal of Superconductivity* **7**, 261 (1994).
- [96] M. Plate, J. D. F. Mottershead, I. S. Elfimov, D. C. Peets, R. Liang, D. A. Bonn, W. N. Hardy, S. Chiuzbaiian, M. Falub, and M. Shi, *Phys. Rev. Lett.* **95**, 077001 (2005).
- [97] I. Tsukada and S. Ono, *Phys. Rev. B* **74**, 134508 (2006).



## SUPPORTING INFORMATION

**Breakdown of scale-invariance below  $T_{\text{co}}$ .** In the present study, we focus on measurements taken in the strange metal phase above  $T_{\text{co}}$  in Fig. 12A. Many previous measurements of the  $T$ -linear resistivity were conducted at low temperatures [23, 32, 93]. Even if the low-temperature resistivity follows a non-Fermi liquid form  $\rho(T) = 1/((\rho_0 + A_1T + A_2T^2)^{-1} + \rho_{\text{max}}^{-1})$ , as suggested in Ref. [32], this expression is not scale-invariant and therefore does not capture the essential features of the strange metal state. Importantly, the resistivity slope  $A_1$  obtained in this regime (‘ $\times$ ’ symbols in Fig. 12B) is significantly reduced relative to that above  $T_{\text{co}}$  with increasing  $p$ , meaning that it is no longer accurately representative of the strange metal state. This contributed to the low value of  $\alpha = 0.9$  at  $p = 0.26$  reported by Legros *et al.* in Ref. [23].

Because earlier studies focused on the resistivity behavior below  $T_{\text{co}}$ , they also required the application of strong magnetic fields to suppress superconductivity. A limitation of these studies—beyond the lack of scale invariance—is that they needed to assume a specific form for the magnetoresistance [32]. In particular, a conventional quadratic form was assumed in Ref. [32], whereas more recent studies have shown the magnetoresistance to be linear [28, 93, 94].

**The specific heat of Tl2201.** Specific heat measurements on  $\text{Tl}_2\text{Ba}_2\text{CuO}_6$  (Tl2201) [95] have been performed over a much narrower range of hole dopings than in LSCO (see Fig. 13A). To compare with these data, we have simulated a curve of the electronic specific heat coefficient  $\gamma$  versus  $p$ , using the doping-dependent band mass  $m$  from Ref. [50]. We first estimate the effective mass  $m^*$  using the empirical relation  $m^*/m = 1.03/p$ , consistent with the dependence obtained in Figs. 3C and D of the main text. We then calculate  $\gamma$  using the expression  $\gamma = m^*(\pi k_{\text{B}}^2 N_{\text{A}} a^2 / 3\hbar^2) \approx (m^*/m_{\text{e}}) \times 1.4 \text{ J mol}^{-1}\text{K}^{-2}$  [50].

Due to the combined effects of the  $1/p$  scaling of  $m^*$  and the fact that the Van Hove singularity occurs at much higher dopings in Tl2201 [96] than in LSCO, the simulated  $\gamma$  shows only a weak dependence on  $p$  over the range where specific heat measurements have been made.

It should be noted that the  $\gamma$  values reported at 200 K by Wade *et al.* [95] were obtained using a differential method, based on the assumption that  $\gamma$  is temperature-independent at the highest doping. Because  $\gamma$  could not be measured directly at 200 K due to the large phonon contribution to the specific heat, a low-temperature value of  $\gamma$  was measured at the highest doping—where superconductivity is absent—and then assumed to hold at 200 K. This procedure introduces a systematic uncertainty in the 200 K data in the form of an offset  $\Delta\gamma$ .

By contrast, in LSCO and Y123, an accurate determination of the phonon contribution was possible because their compositions can be tuned to reach  $p = 0$ , where  $\gamma = 0$  in the antiferromagnetic phase, and also through Zn substitution, which suppresses electronic correlations [49].

Thus, the 200 K  $\gamma$  values for Tl2201 should be regarded as *differential measurements*, subject to a uniform systematic uncertainty across all doping levels. Notably, these differentially obtained values lie below those inferred from magnetic quantum oscillations and the calculated curve in Fig. 13A. If we allow for a uniform shift  $\Delta\gamma \approx 2 \text{ mJ mol}^{-1}\text{K}^{-2}$ , the weak doping-dependence of the observed specific heat data can be brought into reasonable agreement with both quantum oscillation results and our simulation in Fig. 13B.

Overall, additional specific heat measurements of Tl2201 across a broader range of hole dopings are needed to clarify the doping dependence of mass enhancement in this system.

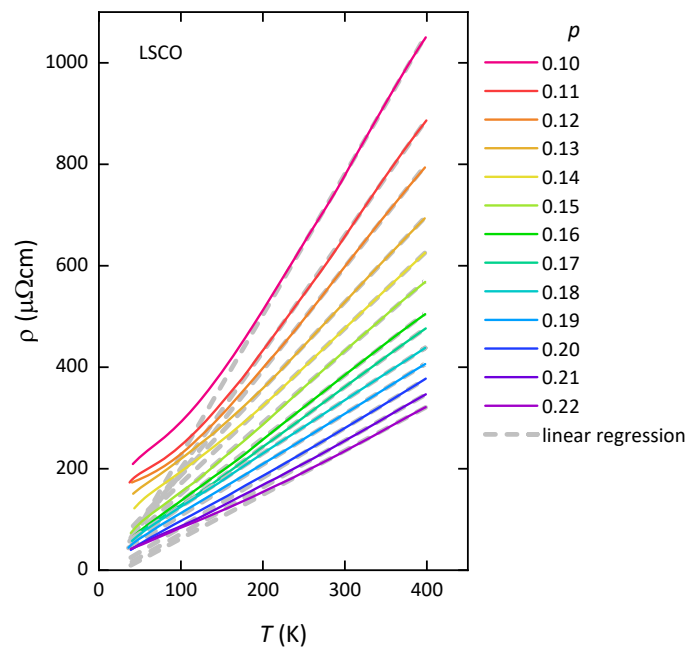


FIG. 6. Measured  $\rho$  versus  $T$  at different hole dopings [15], as indicated in different colors. Dashed lines indicate fits to determine  $A$ . The obtained values of  $1/A$  are plotted in Fig. 1B of the main text.

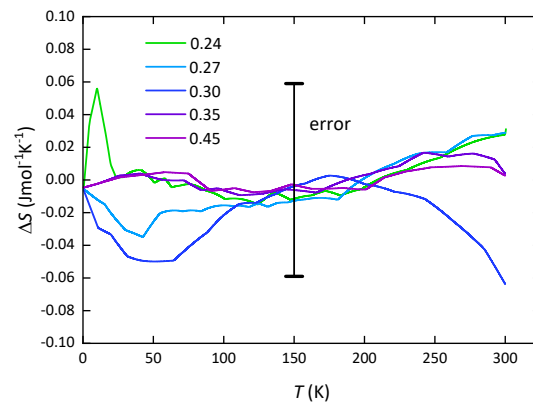


FIG. 7. Difference  $\Delta S$  between the measured and calculated entropy in Figs 3A and B of the main text. The different colors refer to the different hole dopings.

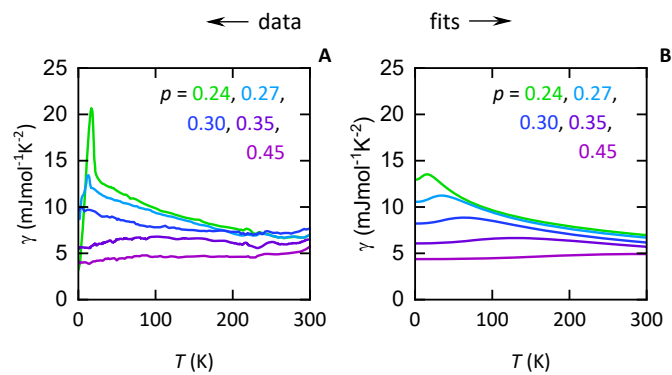


FIG. 8. (A) Measured electronic coefficient  $\gamma$  of the specific heat. (B) Calculated  $\gamma$  versus  $T$  curves using fitted values of  $m/m^*$ .

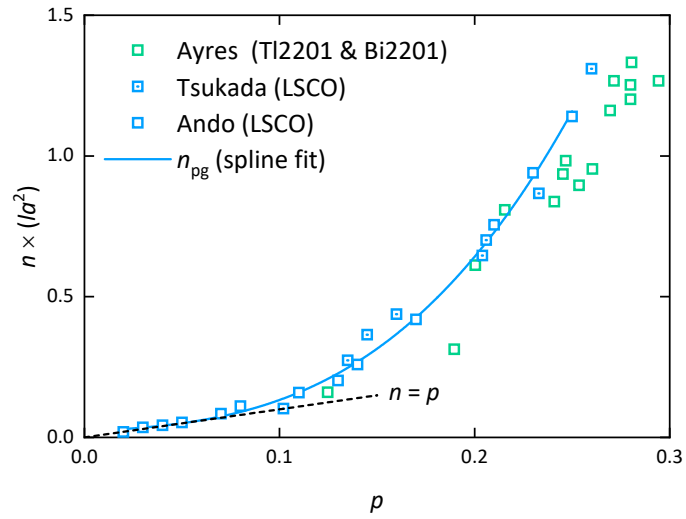


FIG. 9. Effective carrier density  $n = 1/eR_H$  inferred from low temperature Hall effect measurements (above  $T_c$ ) [56, 57, 97].

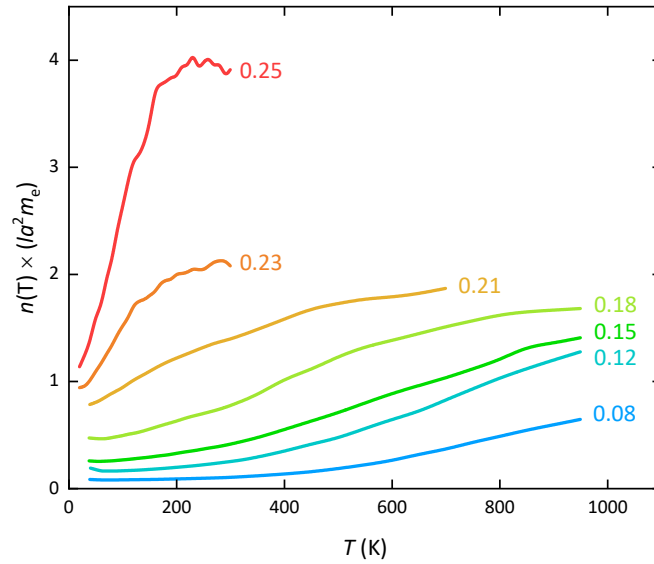


FIG. 10. Value of  $n(T)$  determined from  $R_H$  versus  $T$  measurements in LSCO at different dopings  $p$  as indicated [57, 74].

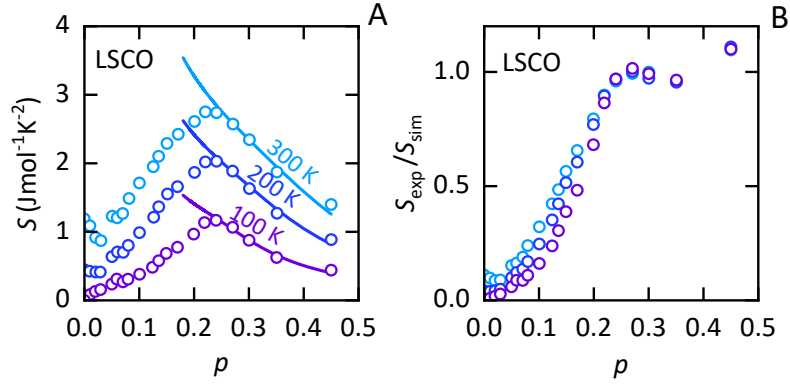


FIG. 11. (A) Measured entropy [48] (circles) at three different temperatures compared to that calculated (solid lines) using  $m/m^* = 1.03 \times p$ . (B), Ratio (circles) of  $S_{\text{exp}}$  (entropy measured) [48] to  $S_{\text{sim}}$  (simulated in (A)).

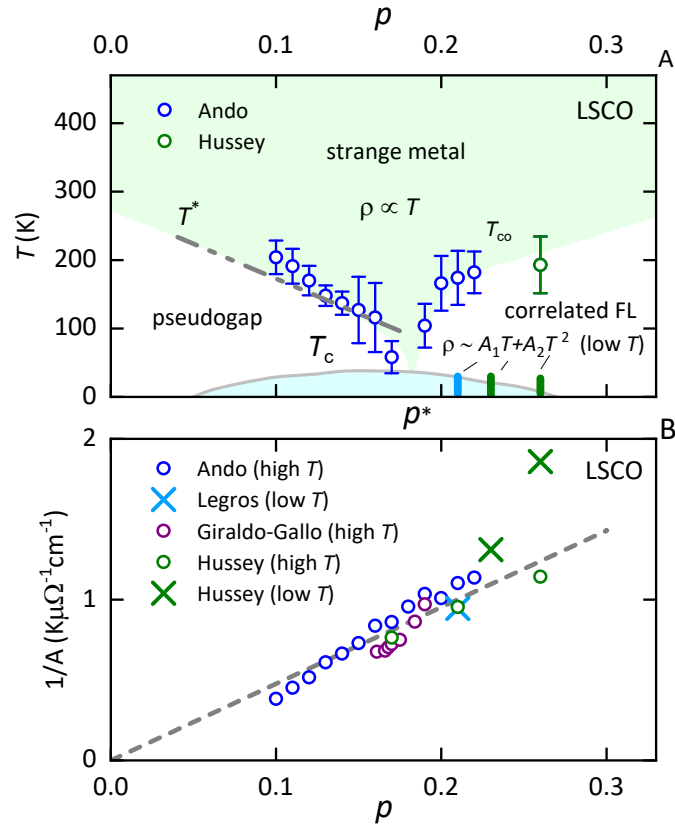


FIG. 12. (A) Same as Fig. 1A from the main text, but with vertical bars added to indicate the low  $T$  range within the non Fermi liquid (FL) regime where the resistivity appears to become linear below  $\approx 30$  K [23]. (B) Same as Fig. 1B from the main text, but with 'x' symbols denoting points obtained at low  $T$  [23, 30].

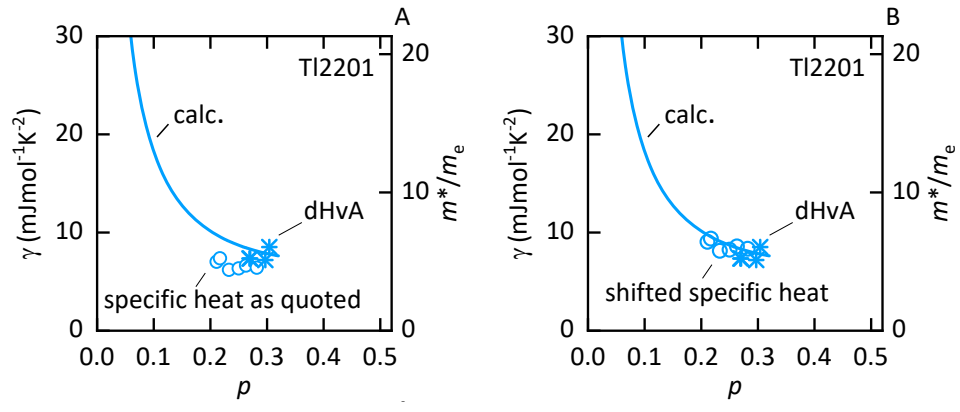


FIG. 13. (A) Calculated specific heat of TI2201 compared with values of  $m^*$  obtained from magnetic quantum oscillation measurements [50] and  $\gamma$  values reported in specific heat experiments [95]. (A) The same plot but with measured values of  $\gamma$  [95] shifted by  $2 \text{ mJmol}^{-1}\text{K}^{-2}$ .